CdSe Quantum-Dot-Sensitized Solar Cell with ~100% Internal Quantum Efficiency

Nobuhiro Fuke,[†,*] Laura B. Hoch,[‡] Alexey Y. Koposov,[‡] Virginia W. Manner,[‡] Donald J. Werder,[‡] Atsushi Fukui,[†] Naoki Koide,[†] Hiroyuki Katayama,[†] and Milan Sykora[‡,*]

[†]New Technology Development Center, Solar Systems Development Group, Sharp Corporation, 282-1 Hajikami, Katsuragi, Nara 639-2198, Japan, and [‡]Physical Chemistry & Applied Spectroscopy, Los Alamos National Laboratory, MS J567, Los Alamos, New Mexico 87545, United States

ABSTRACT We have constructed and studied photoelectrochemical solar cells (PECs) consisting of a photoanode prepared by direct deposition of independently synthesized CdSe nanocrystal quantum dots (NQDs) onto a nanocrystalline TiO_2 film (NQD/TiO_2), aqueous Na_2S or Li_2S electrolyte, and a Pt counter electrode. We show that light harvesting efficiency (LHE) of the NQD/TiO_2 photoanode is significantly enhanced when the NQD surface passivation is changed from tri-*n*-octylphosphine oxide (TOPO) to 4-butylamine (BA). In the PEC the use of NQDs with a shorter passivating ligand, BA, leads to a significant enhancement in both the electron injection efficiency at the NQD/TiO_2 interface and charge collection efficiency at the NQD/electrolyte interface, with the latter attributed mostly to a more efficient diffusion of the electrolyte through the pores of the photoanode. We show that by utilizing BA-capped NQDs and aqueous Li_2S as an electrolyte, it is possible to achieve ~100% internal quantum efficiency of photon-to-electron conversion, matching the performance of dye-sensitized solar cells.

KEYWORDS: nanocrystals · quantum dots · solar cell · quantum-dot-sensitized solar cell · dye-sensitized solar cell · photoelectrochemical solar cell · cadmium selenide

Photoelectrochemical cells (PECs) based on a mesoporous nanocrystalline TiO_2 film (TiO_2 film) sensitized with organic or organometallic dyes have been studied intensely for the past 20 years as a potential low cost alternative to more traditional, solid state photovoltaics.[1,2] Significant progress has been made in optimization of the components of the dye-sensitized solar cell (DSSC) with highest reported efficiencies currently exceeding 11%.[3,4] As part of a search for new approaches to further improvement in efficiency over the past several years, a number of research groups reported studies of PECs in which the sensitizing dyes are substituted with nanocrystals of narrow band gap semiconductors, such as InP,[5] CdS,[6−10] CdSe,[11−13] CdTe,[14] PbS,[15,16] and InAs,[17] also called nanocrystals quantum dots (NQDs). In these studies it was demonstrated that NQDs can function as efficient sensitizers across a broad spectral range from the visible to mid-infrared and offer advantages such as the tunability of optical properties and electronic structure by simple variation in NQD size, while retaining the appeal of low-cost fabrication. In addition, as was demonstrated recently,[18,19] NQDs, of certain materials have the ability to efficiently convert the energy of a single photon into multiple electron−hole pairs *via* a process called carrier multiplication (CM) or multiple exciton generation (MEG). Provided that carriers generated by the MEG effect can be effectively extracted from NQDs, this process has the potential to significantly improve the efficiency of solar cells.[20,21]

Two distinct approaches to the sensitization of TiO_2 film with narrow band gap semiconductors have been demonstrated in recent studies. In one approach, NQDs are generated on the surface of TiO_2 films *in situ*, using chemical bath deposition (CBD)[16,22,23] or successive ionic layer adsorption and reaction (SILAR).[24,25] The advantages of the *in situ* deposition approaches are their simplicity, the fact that the NQDs are in direct electronic contact with TiO_2, and that they can easily produce TiO_2 films with high surface coverage of the sensitizing NQDs. However, there are several limitations of the *in situ* approaches, such as poor control over NQDs chemical composition, crystallinity, size, and surface properties, which may hamper effective exploitation of the advantages of the NQDs.

An alternative approach is based on a two-step process, whereby NQDs are first independently synthesized using established colloidal synthesis methods and the TiO_2 film is subsequently sensitized by exposure to a concentrated solution of the NQDs. The advantage of this approach is a significantly higher control over the chemical, structural, and electronic properties of the NQDs compared to the *in situ*

*Address correspondence to fuke.nobuhiro@sharp.co.jp, sykoram@lanl.gov.

Received for review April 17, 2010 and accepted October 11, 2010.

Published online October 20, 2010. 10.1021/nn101319x

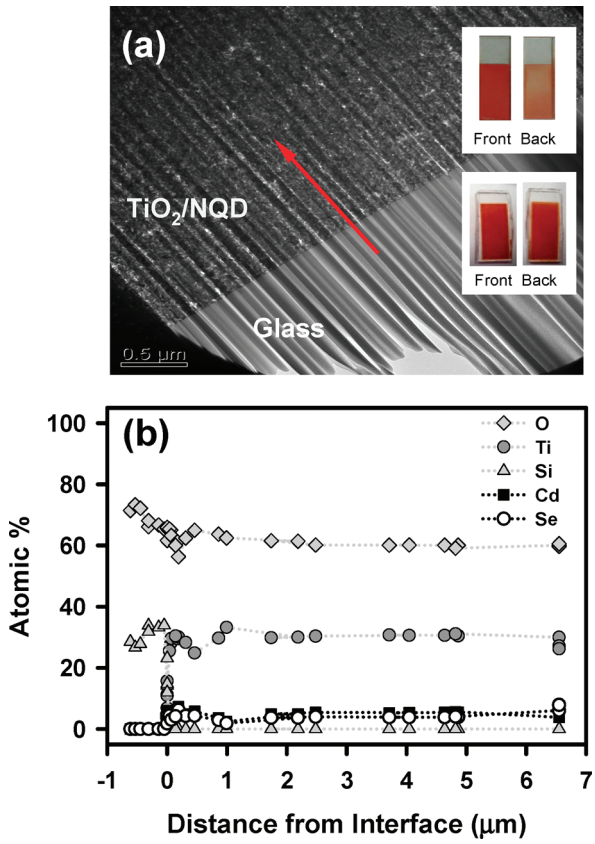

Figure 1. (a) TEM image of the CdSe NQD/TiO_2 film slice cut with a focused ion beam (FIB): slice thickness, 20−180 nm; TiO_2 film thickness, ~6.5 μm; TiO_2 NC size, ~20 nm; NQD radius, ~5.0 nm. The red arrow indicates the direction of the EDS scan shown in panel b. The inset shows digital images of the front and back of CdSe NQD/TiO_2 films deposited on glass. Top image: TiO_2 film thickness, ~20 μm; TiO_2 NC size, ~400 nm; NQD radius, ~5.0 nm. Bottom image: TiO_2 film thickness, ~7 μm; TiO_2 NC size, ~20 nm; NQD radius, ~5.0 nm. (b) EDS analysis of CdSe NQD/TiO_2 film slice shown in panel a. The EDS spectra for each element were taken with respect to the SiO_2/TiO_2 interface (zero point on the abscissa). Thus, the absolute value of negative distance is the distance measured from the interface into the SiO_2 layer. The diameter of CdSe NQDs (including TOPO ligand) is ~7 nm, and the average pore diameter of the TiO_2 film measured by Brunauer Emmett and Teller (BET) method is ~18 nm.

approaches. However, since NQDs, unlike dyes, do not possess an anchoring functional group for coupling to the TiO_2 surface, this approach provides limited control over the TiO_2 sensitization process and degree of NQD-TiO_2 electronic coupling. In addition, NQDs as prepared are typically passivated with a layer of organic ligands, such as tri-*n*-octylphosphine oxide (TOPO), aliphatic amines, or acids, which serve as a impediment to effective TiO_2 sensitization and as a barrier to efficient charge transfer across the NQD/TiO_2 and NQD/electrolyte interfaces. Nevertheless, several groups have demonstrated that exposure of "bare" TiO_2 films or TiO_2 films functionalized with bifunctional organic linkers to concentrated solutions of NQDs leads to their effective sensitization.[5,26−28] While in the studies of PEC performance, several parameters, such as NQD size,[29] type of bifunctional organic linker[28,30] and counter electrode material,[28,31] have been evaluated, the role of NQD organic surface passivation remained mostly unexplored.

In the present work we study how modification of NQD surface passivation affects the performance of PECs utilizing a photoanode prepared by direct deposition of presynthesized CdSe NQDs onto a nanocrystalline TiO_2 film. By performing comparative studies of devices based on NQDs capped with TOPO and with 4-butylamine (BA), we show that the reduction in the length of the passivating ligand leads to significant improvement in light harvesting efficiency (LHE) of the NQD/TiO_2 photoanode and improvement in charge injection and charge collection efficiencies of the PEC device. In PEC devices utilizing BA-capped NQDs and aqueous Li_2S electrolyte, we observe ~100% internal quantum efficiency of photon-to-electron conversion.

RESULTS AND DISCUSSION

Structural and Optical Properties of NQD/TiO_2 Films. The NQDs used in this study were synthesized and purified following a standard literature procedure.[32] The CdSe NQD/TiO_2 composite films were prepared by direct deposition of NQDs onto freshly prepared TiO_2 films from hexane or toluene solution (see Methods section for more details). We find that NQDs effectively infiltrate in and deposit within the pores of TiO_2 as evidenced by significant coloration (Figure 1a inset) and by the appearance of characteristic absorption features of NQDs in the spectra of the films (Figure 2a). This is consistent with previous literature reports.[33] The amount of deposited NQDs, as monitored by absorption spectroscopy, increases with NQD concentration and duration of TiO_2 film soaking with a plateau reached at NQD concentrations of ~10^{-6}−10^{-5} M and exposure time of ~48 h.

One important question from the standpoint of practical application of NQD/TiO_2 composite films in (PECs) is the uniformity of the NQD distribution within the film. In our studies of TiO_2 films with thicknesses between ~5−20 μm we noticed a distinct coloration difference between the front and back face for films with thicknesses >10 μm (Figure 1a inset, top), suggesting limited penetrability of the NQDs into the film. The ~10 μm threshold was not significantly affected by variation in size of TiO_2 nanocrystals (20−400 nm) or the size of NQDs (~4−7 nm). For the films with thicknesses <7 μm there was no observable coloration difference between the front and back face (Figure 1a inset, bottom), suggesting complete penetration of the NQDs across the TiO_2 film. To obtain more detailed information about the NQD distribution in the sub-7 μm films, a thin (20−180 nm) slice of the NQD/TiO_2 composite film, cut with a focused ion beam (FIB), was analyzed by energy dispersive X-ray spectroscopy (EDS). The transmission electron microscope (TEM) image of the slice is shown in Figure 1a, and the results of the EDS elemental analysis of the NQD/TiO_2 slice are shown in Figure 1b. A nearly constant concentration of Cd and Se at-

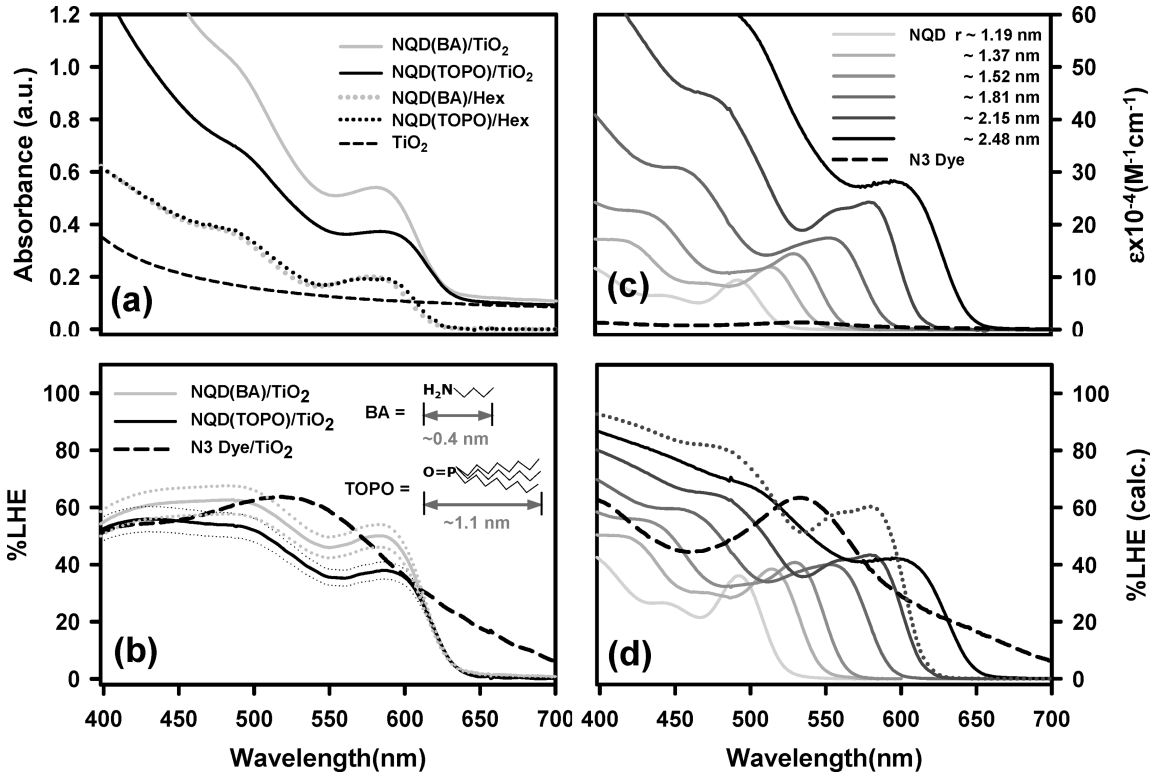

Figure 2. (a) Absorption spectra of CdSe NQDs ($r \sim 2.15$ nm), with 4-butylamine (BA) or tri-*n*-octylphosphine oxide (TOPO) passivation, deposited on TiO_2 films, (film thickness, ~5 μm) and suspended in hexane solution. The NQD/TiO_2 films were prepared by exposure of the TiO_2 film to 3.0×10^{-6} M hexane solution of NQDs for 48 h. Also shown is the absorption spectrum of the blank TiO_2 film. (b) Experimentally determined light harvesting efficiency (LHE) for the two films shown in panel a compared with that of the TiO_2 film of the same thickness sensitized with N3 dye. The dotted lines represent the error of the measurement for the independently prepared films following the same procedure. The TiO_2 film sensitized with an N3 dye was prepared by exposure of the TiO_2 film to 0.3 M solution of the dye in ethanol for 48 h. (c) Molar extinction coefficients of CdSe NQDs (TOPO) of various sizes compared with molar extinction coefficient of N3 dye. (d) Calculated LHE for the same series of CdSe NQDs (TOPO) as in panel c assuming size-scaled surface coverage to be the same as for the N3 dye, shown as a dashed line. The dotted line represents calculated LHE for CdSe NQDs with BA as a passivating ligand.

oms throughout the film indicates that the NQDs not only penetrate all the way to the interface between TiO_2 and glass, but they are also uniformly distributed across the TiO_2 film.

Optical studies of NQD/TiO_2 films revealed that the amount of NQDs deposited within the TiO_2 film is significantly affected by the type of NQD surface passivation (see Figure 2a,b). Figure 2a compares absorption spectra of CdSe NQD/TiO_2 films prepared using NQDs capped with TOPO and films prepared using NQDs capped with BA. The BA-capped CdSe NQDs (NQD(BA)) were prepared from the same batch of TOPO-capped CdSe NQDs (NQD(TOPO)) by sequential precipitation in MeOH and dissolution of NQDs in BA at elevated temperature (see Methods section for details). Also included in Figure 2a are absorption spectra of the same NQDs in hexane solution and the absorption spectrum of the TiO_2 film. Comparison of the spectral features indicates that the modification of surface passivation or adsorption of NQDs into the TiO_2 film does not significantly alter their electronic structure. However, for NQD(BA) we have consistently observed significantly higher optical densities of the NQD/TiO_2 films. This is consistent with the results of light harvesting efficiency (LHE) measurements summarized in Figure 2b, showing clear enhancement of LHE for the NQD(BA). Also included in Figure 2b is the LHE of a TiO_2 film sensitized with an organometallic chromophore cis-di(thiocyanato)-bis(2,2-bipyridyl-4,4-dicarboxylate) ruthenium(II), known as N3 dye. An analysis of the LHE values for the N3/TiO_2, NQD-(TOPO)/TiO_2, and NQD(BA)/TiO_2 provides important insights about the effect of the NQD surface passivation on the optical properties of the NQD/TiO_2 films.

As a first step in our analysis we compare the experimentally determined molar extinction coefficient of N3 dye[34] with the estimated molar extinction coefficients of CdSe NQDs. As was shown previously,[35] the size dependent absorption cross sections of CdSe NQDs at 400 nm can be estimated using an empirical relationship $\sigma_o(cm^2) = (n_{CdSe}/n_{solvent})1.6 \times 10^{-16}\,[r\ (nm)]^3$, where σ_o is an absorption cross section, n_{CdSe} and $n_{solvent}$ are refractive indexes of CdSe NQD (taken as 2.5)[36] and solvent ($n_{hexane} = 1.354$) and r is the NQD radius. The radius of an NQD can be estimated from the absorption spectrum of the NQD solution using an empirical relationship between the NQD size and its band gap, typi-

cally taken as the peak of the lowest energy electronic transition (1s).[35] To convert the calculated value of σ_o (cm^2) to molar extinction coefficient, ε (M^{-1} cm^{-1}), we use the relationship $\varepsilon = \sigma_o N_A/(1000 \times 2.303) = \sigma_o(2.61 \times 10^{20})$, where N_A is the Avogadro's constant. The comparison of calculated values of ε for CdSe NQDs of several sizes and the molar extinction coefficient of N3 dye shows that on a molar basis NQDs are significantly better absorbers than the dye (Figure 2c). This feature makes NQDs a very appealing alternative to molecular dyes as the sensitizer in PECs. However, since NQDs are typically much larger than dyes, the amount of NQDs adsorbed per unit of TiO_2 surface area can be significantly smaller than that of dyes. Therefore the comparison of LHEs in composites with similar chromophore surface coverage is more useful from the practical standpoint.

As was shown previously,[37] in cases when the scattering and the reflectance are small compared to the absorption losses, the LHE is directly related to the molar extinction coefficient of a chromophore as shown in eq 1:

$$\mathrm{LHE}(\lambda) = 1 - 10^{-[1000(cm^3 \cdot L^{-1})\varepsilon(mol^{-1} \cdot L \cdot cm^{-1})\Gamma(mol \cdot cm^{-2})]} \quad (1)$$

In eq 1 the ε is a molar extinction coefficient and Γ is the chromophore surface coverage in mol/cm^2. The calculated LHE for the N3 Dye is shown as a dashed line in Figure 2d. In the calculation we have adjusted the surface coverage so as to match the calculated value of LHE at 525 nm with the experimentally observed value of LHE at the same wavelength (Figure 2b). (Note that the experimentally observed LHE is broadened and partially distorted at high energies due to high TiO_2 absorption). To estimate the maximum achievable LHE by NQDs under the same conditions, we scale the NQD surface coverage using the relationship $\Gamma_{NQD} = \Gamma_{N3}(S_{N3}/S_{NQD})$, where S_{N3} and S_{NQD} are cross-sectional surface areas of N3 dye and the NQDs, respectively. Each value is calculated as $S = \pi \times r^2$, where r_{N3} was taken as 0.58 nm[38] and r_{NQD} was taken as the radius of the NQD plus the length of the ligand (estimated as 1.1 nm for TOPO and 0.4 nm for BA). In this calculation it is assumed that the capping ligands are "impenetrable"; that is, the periphery-to-periphery distance between the NQDs is equal to twice the ligand length. The results of the calculation for TOPO-capped NQDs of several sizes are shown in Figure 2 in solid lines. Also, shown is the result of a calculation for the NQDs with a particle radius of 2.15 nm, capped with BA (dotted line).

The results of the LHE calculations in Figure 2d and their comparison with the experimental LHE shown in Figure 2b yield several insights. First, after accounting for their size, in spite of significantly higher molar extinction coefficients of NQDs compared to N3 dye, NQDs are not significantly better absorbers than molecular dyes, at least at energies close to the band edge. Second, both the theoretical analysis (Figure 2d) and the experiment (Figure 2b) indicate that reduction in length of the NQD capping ligand can significantly improve the LHEs of the NQD/TiO_2 films. Finally, the high LHEs observed experimentally for the NQDs suggest that they effectively cover the TiO_2 surface.

Determination of IPCE in CdSe NQD/TiO_2 PEC. One of the characteristics of the liquid electrolyte-based DSSCs is slow recombination of electrons in TiO_2 films with a redox couple in the electrolyte.[39,40] As a result, in an irradiated device under open circuit conditions, electrons often accumulate in the TiO_2 film. Because of the large surface area of the TiO_2 film this effect is more pronounced in DCCSs than in Shottky-type devices. When the photocurrent measurement is initiated the accumulated charges are released and depending on measurement conditions this can result in overestimation and/or poor reproducibility of the measured photocurrent.[41] The severity of the problem can be usually quantified by systematic studies of photocurrent dependence on measurement conditions, such as measurement integration time and delay time using devices fabricated under the same conditions.[41] In the present work, we observed that the measured values of IPCE are strongly dependent on the specifics of the photocurrent data collection process. Figure 3a shows the results of the IPCE measurements for a PEC based on the CdSe NQD(BA)/TiO_2 photoanode, using various photocurrent integration times. The temporal diagram of the experiment is shown in Figure 3b. As is apparent from Figure 3a, short integration times lead to observation of unreasonably high values of IPCE, but they are reduced as the integration time is increased.

To identify the cause of the variations in the IPCE values, we performed wavelength dependent transient photocurrent measurements. The results summarized in Figure 3c reveal that the highest value of photocurrent is observed immediately upon the start of current data collection (60 ms time resolution) and gradually decreases over time. They also show that the magnitude of the transient photocurrent is wavelength independent. The photocurrent transient reaches plateau approximately after ~3 s. Similar dynamics of transient photocurrent were previously observed in PECs based on dye-sensitized TiO_2,[41−43] where it was attributed to a high capacitance at the TiO_2 film/electrolyte interface resulting from the high surface area of the interface and a slow recombination of the electrons in TiO_2 with the electrolyte redox couple. Given the similarity in the structure of the interface in the NQD/TiO_2 PECs and dye-sensitized PECs (DSSC), it is reasonable to assume that the high capacitance of the NQD-TiO_2 interface is also the primary reason for the significant enhancement of the transient photocurrent on the subsecond time scales observed in our studies. In addition, since the

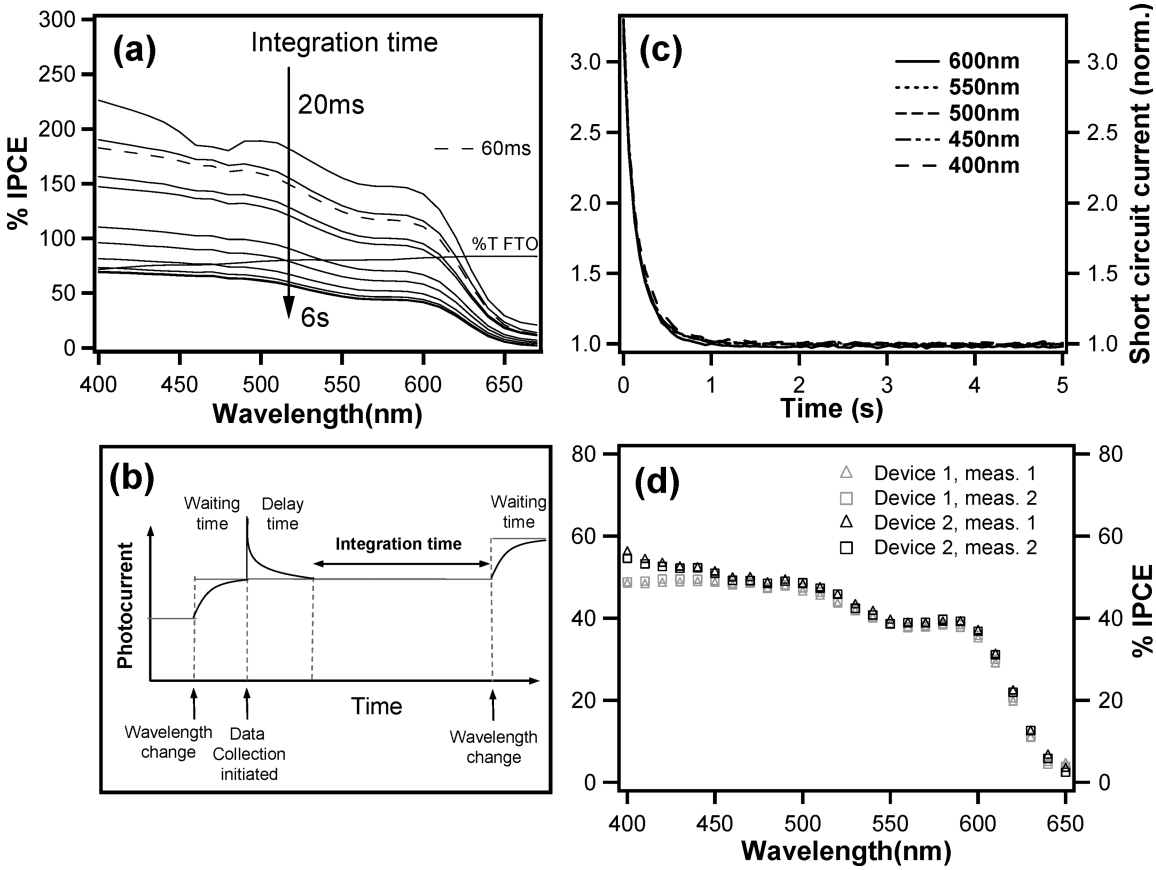

Figure 3. (a) The dependence of incident photon to current conversion efficiency (IPCE) on integration time of the IPCE measurement between 20 ms and 6 s. The IPCE measurement was carried out with a 1 s waiting time and 0 s delay time (see panel b) using CdSe NQD(BA)/TiO_2 photoanode with 1 M aqueous Li_2S electrolyte. The dashed line is the IPCE result obtained with 60 ms integration time, corresponding to time resolution of the photocurrent measurements shown in panel c. (b) A temporal diagram of the IPCE measurement. (c) Transient short circuit current as a function of time under monochromatic light irradiation at several wavelengths using the same device as in panel a. The currents were normalized at 10 s. The instrument time resolution was 60 ms. (d) A comparison of IPCE measurements for two independently fabricated devices using delay time of 3 s and the integration time of 1 s.

electrolyte in NQD PECs contains only the reducing agent, S^{2-} (corresponding to I^- in DSSCs), but no corresponding oxidizing agent (I_3^- in DSSCs), the recombination of electrons in TiO_2 with the redox electrolyte couple may be much slower in NQD PECs. This effect may lead to additional enhancement of the transient photocurrent. To avoid any potential distortions in all our photocurrent measurements, we have introduced a data collection time delay, as shown schematically in Figure 3b. We found that upon introduction of a delay time of ~3 s (to avoid overestimation of photocurrent), and using an integration time of ~1 s (to avoid distortions due to light intensity fluctuation), the IPCE measurements were highly reproducible. Under these conditions, typical variations in IPCE values were less than 5% between measurements, as well as between multiple devices fabricated using the same experimental conditions (Figure 3d).

Effect of Surface Passivation on Short-Circuit Current and Mass Transport in CdSe NQD/TiO_2 PEC. In Figure 4 we show experimentally observed short circuit current (I_{sc}) *versus* irradiation light intensity for two CdSe NQD/TiO_2 PECs prepared under identical conditions, differing only in the type of NQD capping layer. In one group of devices we used NQDs capped with TOPO and in the second the TOPO capping layer was substituted with BA prior to the device fabrication (see Methods section for details). In both groups of devices we observe a nearly linear increase in I_{sc} with increase in irradiation intensity, which is expected according to[34]

$$I_{sc}(\text{mA}) = \int_{\lambda} I_0(\text{mW}) \frac{\lambda(\text{nm})}{1240\ \text{eV/nm}} \text{IPCE}(\lambda)\, d\lambda$$

$$\text{IPCE}(\lambda) = \%T(\lambda)(\text{substrate}) \times \text{LHE}(\lambda) \times \phi_{inj} \times \phi_{coll} \quad (2)$$

In eq 2, I_0 is the incident light intensity at wavelength λ, $\%T(\lambda)$ (substrate) is the transmittance of the substrate at the incident wavelength, ϕ_{inj} is the electron injection efficiency, and ϕ_{coll} is the charge collection efficiency including contributions from electron transport in the TiO_2 film and the redox couple mediated hole transport between the sensitizer and the counter electrode.

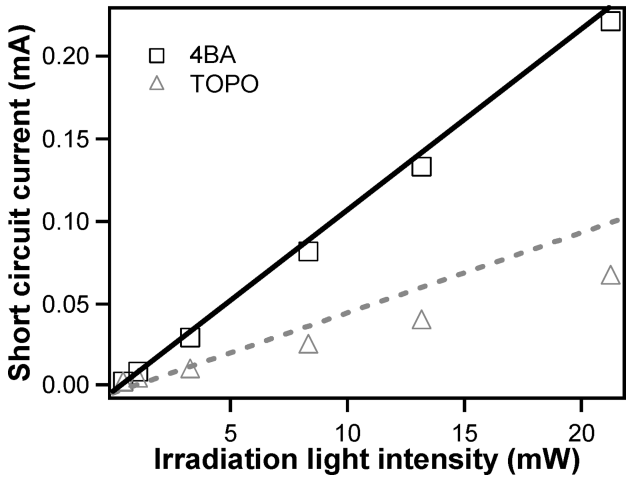

Figure 4. The dependence of short circuit current on the intensity of light irradiation measured using 4-butylamine (BA)-capped (square) and tri-*n*-octylphosphine oxide (TOPO)-capped (triangle) quantum dot-sensitized solar cell with aqueous 1 M Na_2S electrolyte. The straight line (solid line, BA; dotted line, TOPO) is a linear fit going from the origin to the first measurement result at the lowest light irradiation intensity. The area of the device was 0.2209 cm^2.

Despite the similarities in the overall trend of the I_{sc} dependence on light intensity in the two devices, there are some notable differences. The most apparent is the disparity in the absolute values of I_{sc} at all irradiation intensities, with significantly higher I_{sc} values observed for NQD(BA). Consistent with eq 2 and the results shown in Figure 2b part of the enhancement can be attributed to the increase in LHEs of the NQD(BA)/TiO_2 films compared to NQD(TOPO)/TiO_2 films. Enhancement in I_{sc} due to better infiltration of NQDs into TiO_2 films with larger pore sizes was previously reported by Gimeénez *et al.*;[31] however, while the TOPO-to-BA substitution leads to ~40% enhancement in LHE at the 1s peak (Figure 2b), the enhancement in I_{sc} is approximately 4-fold (Figure 4). This indicates that there is an additional factor, besides LHE, that contributes to the I_{sc} enhancement in NQD(BA)-based devices. We propose that the I_{sc} enhancement in NQD(BA) devices is associated with enhancement in charge collection efficiency, whereby the use of shorter BA ligands allows better diffusion of electrolyte through the pores of the NQD/TiO_2 film as well as better access of S^{2-} to the NQD surface. This hypothesis is supported by the observed deviation of the experimental values of I_{sc}, indicated by open squares and open triangles for NQD(BA) and NQD(TOPO), respectively, from the line drawn between the axes origin and the first experimental data point observed at the lowest irradiation intensity. In the case of the NQD(BA) the deviation between the experimental points and the linear line is small, indicating that charge collection efficiencies are not subject to mass transport limitations even at high light intensities. However, for the NQD(TOPO)-based devices the experimental short circuit current values clearly deviate from the linear plot at high light intensities, suggesting increasing mass transport limitations, which we attribute to restricted electrolyte diffusion and NQD surface accessibility.

Effect of Electrolyte and Extent of NQD Adsorption on the IPCE. In Figure 5a,b we show a summary of the IPCE studies for a series of CdSe NQD/TiO_2 PECs prepared using different NQD ligand capping (TOPO, BA), concentration of the NQD solution (3×10^{-5}, 3×10^{-6} M) used for TiO_2 infiltration, and electrolyte (aqueous Na_2S, Li_2S). An example of the experimentally measured $I-V$ curves for the devices based on TOPO-capped and BA-capped NQDs is shown in the Supporting Information. Consistent with the results of short circuit current measurements discussed in the previous section, measured IPCEs are significantly smaller for NQD(TOPO) than NQD(BA), regardless of the type of electrolyte or the concentration of the NQD solution used for TiO_2 infiltration. For the NQD(BA) we find that the IPCE increases with the concentration of the NQD solution, which we attribute to the enhancement in the LHE. Interestingly, in the case of TOPO-capped NQDs the increase in the concentration of the NQD solution does not lead to IPCE enhancement. In fact, when Li_2S electrolyte is used (Figure 5b), an increased concentration of TOPO-capped NQDs leads to IPCE reduction. Since the LHE increases with the concentration of the NQD solution, the observed reduction in IPCE suggests suppressed charge injection or collection efficiencies. This could be caused either by nonuniform infiltration of NQDs into the TiO_2 film and/or by restricted diffusion of a redox couple into the TiO_2 film loaded with large amount of NQDs.

For the BA-capped NQDs we observe higher IPCE values with Li_2S electrolyte (Figure 5a) compared to Na_2S electrolyte (Figure 5b). In an independent measurement (data not shown) we have also observed that open circuit voltage (V_{oc}) of devices with Li_2S electrolyte was reduced compared to Na_2S electrolyte. In the case of DSSCs, it was shown that a decrease in V_{oc} can be closely correlated with a shift in the TiO_2 conduction band to more positive values.[44−46] This effect was explained in terms of Li^+-induced changes in the TiO_2 electronic structure.[47] Since the electronic structures of the dyes are typically unaffected by the cation of the electrolyte, the positive shift of the TiO_2 conduction band leads to an increase in the driving force for the dye → TiO_2 electron transfer, which in turn leads to enhanced electron injection efficiencies and consequently higher IPCEs.[44−46] On the basis of our observation of reduced V_{oc} in NQD PCEs studied here we propose that the enhancement in IPCEs observed in the presence of Li_2S electrolyte is due to a similar effect. The good overlap between the 1s peak feature observed in LHE and IPCE measurements suggests that the electronic structure of the NQDs is not significantly affected by the presence of electrolyte. Therefore, the positive shift of the TiO_2 conduction band likely leads to an increase in the energy offset between the NQD and TiO_2 conduc-

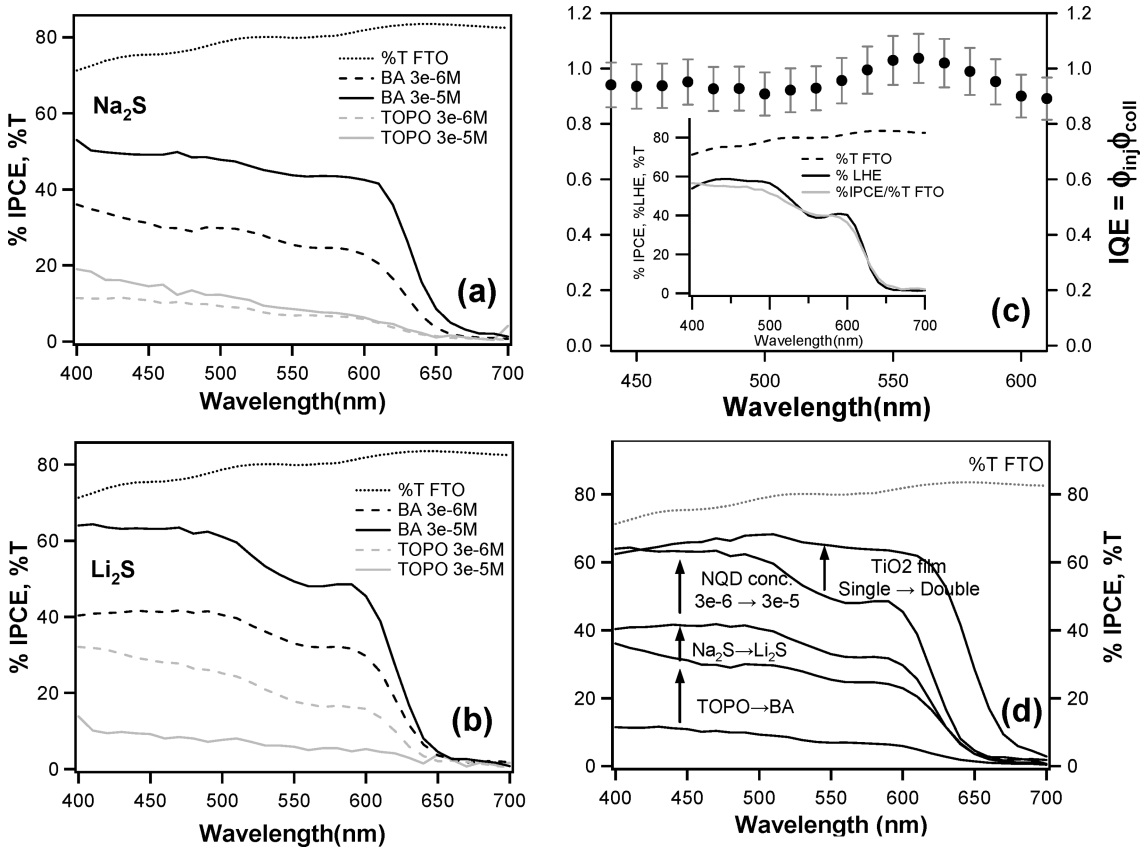

Figure 5. Incident photon-to-current conversion efficiency (IPCE) for CdSe NQD/TiO_2 solar cells using NQDs with 4-butylamine (BA) or tri-*n*-octylphosphine oxide (TOPO) as capping ligands and different concentrations of solutions used for TiO_2 infiltration. The electrolyte was in (a) 1 M Na_2S and in (b) 1 M Li_2S aqueous solution. (c) The dependence of IQE (internal quantum efficiency) calculated as: IQE = (IPCE/%*T* FTO)/% LHE. Inset: The experimental data used for calculation of IQE of the device shown in solid circles in the main panel. (d) Dependence of IPCE on various device preparation conditions. The absorption spectrum increases at all wavelengths due to the significant change in path length from a single-layer TiO_2 film to a double-layer film.

tion bands, thus increasing the driving force for the NQD-TiO_2 electron injection. Improvement in electron injection efficiency is then reflected in the enhanced IPCEs.

In the case of NQD(TOPO) devices prepared with lower concentration of NQD solutions, the use of Li_2S led to a more significant enhancement in IPCE than for NQD(BA) devices. With the application of the arguments discussed in the previous section this result suggests that the Li^+-induced shift in the TiO_2 conduction band offset has a much more pronounced effect on the electron injection efficiency from TOPO-capped NQDs. Although the exact reason for this is not known, we speculate that in the case of TOPO ligands the activation barrier for the NQD→TiO_2 electron transfer is larger and is more sensitive to small variations in the free energy change associated with the electron transfer process.

Determination of Internal Quantum Efficiency (IQE) for the CdSe NQD/TiO_2 PEC. IQE is an important characteristic of a PEC, indicating how efficiently the absorbed (rather than incident) photons are converted to current in the external circuit. For IQE = 1, every photon absorbed by an active medium of the solar cell is converted to current. The IQE of the PEC can be estimated from experimentally determined IPCE and LHE, after accounting for losses due to light absorption by the FTO substrate, according to[34]

$$\mathrm{IQE} = \mathrm{IPCE}/(\%T(\mathrm{FTO}) \times \mathrm{LHE}) = \phi_{\mathrm{inj}} \times \phi_{\mathrm{coll}} \qquad (3)$$

The results of the IQE analysis for the NQD(BA)/TiO_2 device prepared using 3×10^{-6} M NQD solution and 1 M aqueous Li_2S as an electrolyte are shown in Figure 5c. The main panel shows the calculated IQE and the inset shows the experimentally measured LHE and IPCE as well as the transmittance of the FTO substrate used in the calculation. We note that the measurement of the IPCE was performed on a PEC device, and the measurement of LHE was performed on TiO_2/NQD film prepared under identical conditions, but in the absence of electrolyte. The results of our analysis show that the IQE of the device is ~100% for the entire spectral range between ~450−600 nm. To our knowledge this is the highest IQE reported for a NQD-based solar cell. As implied by eq 3 the high IQE indicates that both electron injection and charge collection efficiencies are nearly 100%. Near 100% electron injection efficiency was reported previously for CdS/TiO_2 composite films pre-

pared by chemical bath deposition.[48] Our results indicate that the interfacial electron transfer and charge transport in the NQD-based PECs prepared here are comparable with the most efficient DSSCs under short circuit conditions. The experimentally measured $I-V$ curves for the device are shown in the Supporting Information.

Effect of TiO_2 Film Structure on the IPCE. To further improve the IPCE of NQD PECs we have fabricated a series of devices using a double layer TiO_2 film structure consisting of a bottom (in contact with FTO) light absorption layer (~5 μm with 20 nm particles) and a top scattering layer (~5 μm with 400 nm particles). This type of structure is commonly used to enhance the LHEs of DSSCs.[3] The results of the IPCE study of the double layer structure compared with different configurations of monolayer devices, using the same size of NQDs (1 s at 590 nm; $r \sim 2.3$ nm) are shown in Figure 5d. The results clearly show enhancement in the IPCE of the double layer device for all wavelengths above 450 nm, which is attributed to the scattering-induced increase in the path length of the incident light. The short circuit current density (J_{sc}) calculated using the measured IPCE and AM 1.5 solar radiation spectrum is 10.2 mA/cm^2, which means that in this device ~65% of all photons transmitted to FTO substrate between 400−700 nm are converted to measured external current (100% corresponds to $J_{sc} = 15.8$ mA/cm^2).

We note that although the peak of the 1s band edge absorption for the NQDs used in the studies of double layer-based devices is at 590 nm, the IPCE value at 650 nm is ~30% (*i.e.*, *ca.* half of the IPCE at 590 nm), and the edge of the detectable IPCE is at ~700 nm. We estimate that by using the larger size CdSe NQDs (radius of ~5 nm, 1s peak at ~650), the edge of IPCE can be extended to ~750 nm. The IPCE edge at this wavelength is approaching the IPCE edge (~800 nm) of DSSCs with N719 (cis-di(isothiocyanato)-bis(2,2′-bipyridyl-4,4′-dicarboxylato)ruthenium(II)-bis(tetrabutylammonium)) dye, which was shown to produce record power conversion efficiencies among the DSSCs (>11%).[3] Provided that the charge injection and transport efficiencies can be maintained, this suggests that PECs with large CdSe NQDs have the potential to achieve short circuit currents competitive with the best DSSCs. While the high IPCEs and IQEs observed in this work are encouraging, the development of CdSe NQD-based PECs with power conversion efficiencies similar to the best DSSCs will require significant effort in development and optimization of a regenerative electrolyte system as well as identification of an optimal counter electrode material, possibly different from Pt[31] used in devices studied in the present work.

CONCLUSIONS

We have investigated optical properties of CdSe NQD/TiO_2 composite films and their applications in PECs. We showed that the reduction in the size of the NQD surface capping ligand can lead to a significant enhancement in the LHE of the composite films due to more efficient coverage of the TiO_2 surface. In PECs the use of shorter capping ligands also leads to a significant enhancement in charge injection and charge collection efficiencies. We demonstrated that ~100% internal quantum efficiency can be achieved in devices utilizing aqueous Li_2S electrolyte, matching the electron injection and charge collection efficiencies of DSSCs.

METHODS

Chemicals. $CdMe_2$ was purchased from Strem Chemicals; tri-*n*-octylphosphine oxide (TOPO) (technical grade, 90%) and tri-*n*-octylphosphine TOP (technical grade, 90%) were purchased from Aldrich (batch no. 06820CH, 07596KJ, respectively); Se shot (99.999%) was purchased from Alfa Aesar; extra dry hexane and methanol were purchased from Acros Organics, 4-butylamine (99%) was purchased from Aldrich.

Synthesis and Purification of CdSe NQDs. The TOPO-capped NQDs were synthesized and purified following a standard literature procedure.[32] All the synthetic and purification steps were performed under Ar atmosphere and the product was stored in an Ar-filled glovebox until use.

NQD Ligand Exchange. All the operations were performed in a glovebox under Ar. The NQD growth solution (1 g) was dissolved in 1.5 mL of hexane at 35 °C. To this solution, 8−10 mLof MeOH was added to precipitate the NQDs. The solution was centrifuged and decanted, and the decanted NQDs were dissolved in 0.5 mL of 4-butylamine. This solution was heated for 40−60 min at 55 °C, poured into a centrifuge tube, and precipitated with 5 mL of MeOH. The solution was centrifuged and decanted, and the precipitate redissolved in 0.5 mL of 4-butylamine. The solution was again heated for 15−30 min at 55 °C and then precipitated with 4 mL of MeOH. The last step was repeated one more time, and the resulting NQDs were dissolved in 0.2 mL of 4-butylamine plus 2 mL of toluene and stored in this mixture for future use.

Preparation of NQD/TiO_2 Films. Nanocrystalline TiO_2 films were prepared using a procedure described previously.[49] For the optical measurements the films were deposited on 1 mm thick glass slides (Marathon Glass), while for the devices the films were deposited onto 1 mm fluorine-doped tin oxide coated glass (F−SnO_2 glass). Following the deposition the films were sintered at 500 °C to remove organic components.[49] The thickness of the films was determined by step-profilometry using Alpha Step 500 Tencor Instruments) profilometer. The NQD/TiO_2 films were prepared by exposing freshly sintered TiO_2 to a solution of TOPO-capped CdSe NQDs in hexane, or 4-butylamine-capped CdSe NQDs in toluene under Ar atmosphere. We note that the deposition of TOPO-capped NQDs onto TiO_2 from toluene solution was significantly less efficient than deposition of NQD-(TOPO) from hexane or NQD(BA) from toluene as evidenced by absorption and LHE measurements. Unless, stated otherwise in text the typical exposure time was 48 h. The NQD/TiO_2 films were washed twice with the appropriate solvent and were allowed to dry under Ar. Dry films were stored in dark in a glovebox under Ar atmosphere until use.

Preparation of TEM Cross-Section. The TEM cross-section was prepared by using an FEI focused ion beam (FIB) system. An ion beam voltage of 30 KV with a current of 3000−5000 pA was used to excavate the foil. Progressively smaller currents (1000 pA

down to 100 pA) was used to thin the foil cross-section. A final cleanup of the TEM cross-section surface was done using a 10 KV, 70 pA beam.

EDS Measurements. The energy dispersive spectroscopy (EDS) was done using a Bruker XFlash detector on a JEOL 2010 TEM operating at 200 KV. EDS spectra in Figure 1b for each element were taken with respect to the SiO_2/TiO_2 interface (zero point on the abscissa). Thus, the absolute value of negative distance is the distance measured from the interface into the SiO_2 layer. To obtain enough counts, X-ray fluorescence was taken at each spot for several minutes in spot mode.

LHE Measurements. The LHE measurements were performed following a literature procedure.[50] The transmittance and reflectance spectra of the NQD/TiO_2 and blank TiO_2 films were collected on a Perkin-Elmer Lambda 950 spectrometer equipped with an integrating sphere and a Si detector. The LHE was calculated using

$$\mathrm{LHE} = [\%T_{\mathrm{TiO_2}} - \%T_{\mathrm{NQD}}] + [\%R_{\mathrm{TiO_2}} - \%R_{\mathrm{NQD}}] \qquad (4)$$

where $\%T_{\mathrm{TiO_2}}$ is the percent transmittance of the TiO_2 film alone, $\%T_{\mathrm{NQD}}$ is the percent transmittance of the NQD/TiO_2 film, $\%R_{\mathrm{TiO_2}}$ is the percent reflectance of the TiO_2 film alone, and $\%R_{\mathrm{NQD}}$ is the percent reflectance of the NQD/TiO_2 film. This procedure neglects scattering and wave guiding effects associated with the FTO substrate, which leads to slight overestimation of LHEs.

Fabrication of PECs. The NQD-based solar cells were fabricated using a two-electrode sandwich cell configuration similar to standard DSSCs arrangement. A platinum-coated F−SnO_2 glass was used as the counter electrode (CE). The two electrodes (a NQD/TiO_2 film on a F−SnO_2 glass and CE) were separated by a Surlyn spacer (40−50 μm thick, DuPont) and sealed by heating the polymer frame. The cell was filled with electrolyte (aqueous 1 M Na_2S or Li_2S) using capillary action.

PEC Devices Characterization. The IPCE measurements were performed using QE/IPCE Measurement Kit equipped with 150 W Xe lamp (no. 6253, Newport) as a light source and Oriel Cornerstone no. 260 $^1/_4$ m monochromator. The light intensity was adjusted with series of neutral density filters and monitored with Newport optical power meter 1830C power meter with calibrated Si power meter, Newport model 818 UV. The photocurrent generated by the device was measured using a Keithley 6517A electrometer. Current voltage ($I-V$) measurements were performed using the same experimental arrangement. To irradiate the sample with a broadband white light instead of monochromatic light, the grating in the monochromator was substituted with a manufacturer supplied high reflectivity broadband silver mirror. A black mask (0.2209 cm^2) was attached to the solar cells in order to prevent irradiation with a scattered light. For both types of measurements the communication between the instruments and the computer was facilitated *via* a GPIB interface, and the instrument control and data processing were performed using software written locally in Labview.

Acknowledgment. This work was supported by Sharp Corporation under the Sharp—Los Alamos National Laboratory CRADA No. 10583.0. M.S., A.Y.K., and V.W.M. acknowledge partial support by the Los Alamos National Laboratory Directed Research and Development Funds. M.S. and D.J.W. acknowledge partial support by the Center for Advanced Solar Photophysics, an Energy Frontier Research Center funded by the U.S. Department of Energy (DOE), Office of Science, Office of Basic Energy Sciences (BES).

Note Added after ASAP Publication: This paper was published on October 20, 2010 with an incorrect author affiliation. The corrected version was published on October 28, 2010. A change to the Acknowledgment was made in the version that reposted November 2, 2010.

Supporting Information Available: I−V characteristics of the devices based on TOPO- and BA-capped CdSe NQDs. This material is available free of charge *via* the Internet at http://pubs.acs.org.

REFERENCES AND NOTES

1. Gratzel, M. Photoelectrochemical Cells. *Nature* **2001**, *414*, 338–44.
2. Gratzel, M. Solar Energy Conversion by Dye-Sensitized Photovoltaic Cells. *Inorg. Chem.* **2005**, *44*, 6841–6851.
3. Nazeeruddin, M. K.; De Angelis, F.; Fantacci, S.; Selloni, A.; Viscardi, G.; Liska, P.; Ito, S.; Takeru, B.; Gratzel, M. Combined Experimental and DFT-TDDFT Computational Study of Photoelectrochemical Cell Ruthenium Sensitizers. *J. Am. Chem. Soc.* **2005**, *127*, 16835–16847.
4. Chiba, Y.; Islam, A.; Watanabe, Y.; Komiya, R.; Koide, N.; Han, L. Dye-Sensitized Solar Cells with Conversion Efficiency of 11.1%. *Jpn. J. Appl. Phys.* **2006**, *45*, L638–L640.
5. Zaban, A.; Micic, O. I.; Gregg, B. A.; Nozik, A. J. Photosensitization of Nanoporous TiO_2 Electrodes with InP Quantum Dots. *Langmuir* **1998**, *14*, 3153–3156.
6. Peter, L. M.; Riley, D. J.; Tull, E. J.; Wijayantha, K. G. U. Photosensitization of Nanocrystalline TiO_2 by Self-Assembled Layers of CdS Quantum Dots. *Chem. Commun.* **2002**, 1030–1031.
7. Tachibana, Y.; Umekita, K.; Otsuka, Y.; Kuwabata, S. Performance Improvement of CdS Quantum Dots Sensitized TiO_2 Solar Cells by Introducing a Dense TiO_2 Blocking Layer. *J. Phys. D* **2008**, *41*, 102002 (5 pp.).
8. Toyoda, T.; Sato, J.; Shen, Q. Effect of Sensitization by Quantum-Sized CdS on Photoacoustic and Photoelectrochemical Current Spectra of Porous TiO_2 Electrodes. *Rev. Sci. Instrum.* **2003**, *74*, 297–299.
9. Vogel, R.; Hoyer, P.; Weller, H. Quantum-Sized PbS, CdS, Ag_2S, Sb_2S_3, and Bi_2S_3 Particles as Sensitizers for Various Nanoporous Wide-Bandgap Semiconductors. *J. Phys. Chem.* **1994**, *98*, 3183–3188.
10. Vogel, R.; Pohl, K.; Weller, H. Sensitization of Highly Porous, Polycrystalline TiO_2 Electrodes by Quantum Sized CdS. *Chem. Phys. Lett.* **1990**, *174*, 241–6.
11. Fang, J. H.; Wu, J. W.; Lu, X. M.; Shen, Y. C.; Lu, Z. H. Sensitization of Nanocrystalline TiO_2 Electrode with Quantum Sized CdSe and ZnTcPc Molecules. *Chem. Phys. Lett.* **1997**, *270*, 145–151.
12. Liu, D.; Kamat, P. V. Photoelectrochemical Behavior of Thin CdSe and Coupled TiO_2/CdSe Semiconductor Films. *J. Phys. Chem.* **1993**, *97*, 10769–10773.
13. Shen, Q.; Arae, D.; Toyoda, T. Photosensitization of Nanostructured TiO_2 with CdSe Quantum Dots: Effects of Microstructure and Electron Transport in TiO_2 Substrates. *Photochem. Photobiol. A* **2004**, *164*, 75–80.
14. Lee, H. J.; Kim, D.-Y.; Yoo, J.-S.; Bang, J.; Kim, S.; Park, S.-M. Anchoring Cadmium Chalcogenide Quantum Dots (QDs) onto Stable Oxide Semiconductors for QD Sensitized Solar Cells. *Bull. Korean Chem. Soc.* **2007**, *28*, 953–958.
15. Hoyer, P.; Konenkamp, R. Photoconduction in Porous TiO_2 Sensitized by PbS Quantum Dots. *Appl. Phys. Lett.* **1995**, *66*, 349–351.
16. Plass, R.; Pelet, S.; Krueger, J.; Gratzel, M.; Bach, U. Quantum Dot Sensitization of Organic−Inorganic Hybrid Solar Cells. *J. Phys. Chem. B* **2002**, *106*, 7578–7580.
17. Yu, P.; Zhu, K.; Norman, A. G.; Ferrere, S.; Frank, A. J.; Nozik, A. J. Nanocrystalline TiO_2 Solar Cells Sensitized with InAs Quantum Dots. *J. Phys. Chem. B* **2006**, *110*, 25451–25454.
18. Ellingson, R. J.; Beard, M. C.; Johnson, J. C.; Yu, P.; Micic, O. I.; Nozik, A. J.; Shabaev, A.; Efros, A. L. Highly Efficient Multiple Exciton Generation in Colloidal PbSe and PbS Quantum Dots. *Nano Lett.* **2005**, *5*, 865–871.
19. Schaller, R. D.; Klimov, V. I. High Efficiency Carrier Multiplication in PbSe Nanocrystals: Implications for Solar Energy Conversion. *Phys. Rev. lett.* **2004**, *92*, 1866011−4.
20. Hanna, M. C.; Nozik, A. J. Solar Conversion Efficiency of Photovoltaic and Photoelectrolysis Cells with Carrier Multiplication Absorbers. *J. Appl. Phys.* **2006**, *100*, 1–8.
21. Klimov, V. I. Detailed-Balance Power Conversion Limits of Nanocrystal-Quantum-Dot Solar Cells in the Presence of Carrier Multiplication. *Appl. Phys. Lett.* **2006**, 89.
22. Diguna, L. J.; Qing, S.; Kobayashi, J.; Toyoda, T. High Efficiency of CdSe Quantum-Dot-Sensitized TiO_2 Inverse Opal Solar Cells. *Appl. Phys. Lett.* **2007**, *91*, 23116/1–3.

23. Tachibana, Y.; Akiyama, H. Y.; Ohtsuka, Y.; Torimoto, T.; Kuwabata, S. CdS Quantum Dots Sensitized TiO_2Sandwich-Type Photoelectrochemical Solar Cells. *Chem. Lett.* **2007**, *36*, 88–89.
24. Li, J. J.; Wang, Y. A.; Guo, W. Z.; Keay, J. C.; Mishima, T. D.; Johnson, M. B.; Peng, X. G. Large-Scale Synthesis of Nearly Monodisperse CdSe/CdS Core/Shell Nanocrystals Using Air-Stable Reagents *via* Successive Ion Layer Adsorption and Reaction. *J. Am. Chem. Soc.* **2003**, *125*, 12567–12575.
25. Lee, H. J.; Moon, S.-J.; Chen, P.; Ito, S.; Zakeeruddin, S. M.; Graetzel, M.; Nazeeruddin, M. K.; Leventis, H. C.; Haque, S. A.; Torres, T.; *et al*. PbS and CdS Quantum Dot-Sensitized Solid-State Solar Cells: "Old Concepts, New Results. *Adv. Funct. Mater.* **2009**, *19*, 2735–2742.
26. Leschkies, K. S.; Divakar, R.; Basu, J.; Enache-Pommer, E.; Boercker, J. E.; Carter, C. B.; Kortshagen, U. R.; Norris, D. J.; Aydil, E. S. Photosensitization of ZnO Nanowires with CdSe Quantum Dots for Photovoltaic Devices. *Nano Lett.* **2007**, *7*, 1793–1798.
27. Lòpez-Luke, T.; Wolcott, A.; Xu, L.-P.; Chen, S.; Wen, Z.; Li, J.; De La Rosa, E.; Zhang, J. Z. Nitrogen-Doped and CdSe Quantum-Dot-Sensitized Nanocrystalline TiO_2 Films for Solar Energy Conversion Applications. *J. Phys. Chem. C* **2008**, *112*, 1282–1292.
28. Mora-Serò, I. n.; Gimènez, S.; Moehl, T.; Fabregat-Santiago, F.; Lana-Villareal, T.; Gòmez, R.; Bisquert, J. Factors Determining the Photovoltaic Performance of a CdSe Quantum Dot Sensitized Solar Cell: The Role of the Linker Molecule and of the Counter Electrode. *Nanotechnology* **2008**, *19*, 424007.
29. Kongkanand, A.; Tvrdy, K.; Takechi, K.; Kuno, M.; Kamat, P. V. Quantum Dot Solar Cells. Tuning Photoresponse through Size and Shape Control of CdSe−TiO_2 Architecture. *J. Am. Chem. Soc.* **2008**, *130*, 4007–4015.
30. Robel, I.; Subramanian, V.; Kuno, M.; Kamat, P. V. Quantum Dot Solar Cells. Harvesting Light Energy with CdSe Nanocrystals Molecularly Linked to Mesoscopic TiO_2 Films. *J. Am. Chem. Soc.* **2006**, *128*, 2385–2393.
31. Gimènez, S.; Mora-Serò, I.; MacOr, L.; Guijarro, N.; Lana-Villarreal, T.; Gòmez, R.; Diguna, L. J.; Shen, Q.; Toyoda, T.; Bisquert, J. Improving the Performance of Colloidal Quantum-Dot-Sensitized Solar Cells. *Nanotechnology* **2009**, *20*, 295204.
32. Murray, C. B.; Norris, D. J.; Bawendi, M. G. Synthesis and Characterization of Nearly Monodisperse CdE (E = S, Se, Te) Semiconductor Nanocrystallites. *J. Am. Chem. Soc.* **1993**, *115*, 8706–8715.
33. Guijarro, N.; Lana-Villarreal, T.; Mora-Sero, I.; Bisquert, J.; Gomez, R. CdSe Quantum Dot-Sensitized TiO_2 Electrodes: Effect of Quantum Dot Coverage and Mode of Attachment. *J. Phys. Chem. C* **2009**, *113*, 4208–4214.
34. Nazeeruddin, M. K.; Kay, A.; Rodicio, I.; Humphry-Baker, R.; Mueller, E.; Liska, P.; Vlachopoulos, N.; Graetzel, M. Conversion of Light to Electricity by *cis*-X_2Bis(2,2′-bipyridyl-4,4′-dicarboxylate)ruthenium(II) Charge-Transfer Sensitizers (X = Cl^-, Br^-, I^-, CN^-, and SCN^-) on Nanocrystalline Titanium Dioxide Electrodes. *J. Am. Chem. Soc.* **1993**, *115*, 6382–6390.
35. Klimov, V. I. Optical Nonlinearities and Ultrafast Carrier Dynamics in Semiconductor Nanocrystals. *J. Phys. Chem. B* **2000**, *104*, 6112–6123.
36. Pankove, J. I. *Optical Processes in Semiconductors*; Dover Publications: New York, 1971.
37. Argazzi, R.; Bignozzi, C. A.; Heimer, T. A.; Castellano, F. N.; Meyer, G. J. Enhanced Spectral Sensitivity from Ruthenium(II) Polypyridyl-Based Photovoltaic Devices. *Inorg. Chem.* **1994**, *33*, 5741–5749.
38. The size of the N3 dye was estimated from a semi-empirical molecular modeling calculation using the commercial Cashe (5.0) ZINDO package (CAChe Group).
39. Han, L.; Koide, N.; Chiba, Y.; Mitate, T. Modeling of an Equivalent Circuit for Dye-Sensitized Solar Cells. *Appl. Phys. Lett.* **2004**, *84*, 2433–2435.
40. Kern, R.; Sastrawan, R.; Ferber, J.; Stangl, R.; Luther, J. Modeling and Interpretation of Electrical Impedance Spectra of Dye Solar Cells Operated under Open-Circuit Conditions. *Electrochim. Acta* **2002**, *47*, 4213–4225.
41. Koide, N.; Han, L. Measuring Methods of Cell Performance of Dye-Sensitized Solar Cells. *Rev. Sci. Instrum.* **2004**, *75*, 2828–2831.
42. Walker, A. B.; Peter, L. M.; Martinez, D.; Lobato, K. Transient Photocurrents in Dye-Sensitized Nanocrystalline Solar Cells. *Chimia* **2007**, *61*, 792–795.
43. Nakade, S.; Kambe, S.; Kitamura, T.; Wada, Y.; Yanagida, S. Effects of Lithium Ion Density on Electron Transport in Nanoporous TiO_2 Electrodes. *J. Phys. Chem. B* **2001**, *105*, 9150–9152.
44. Furube, A.; Katoh, R.; Hara, K.; Sato, T.; Murata, S.; Arakawa, H.; Tachiya, M. Lithium Ion Effect on Electron Injection from a Photoexcited Coumarin Derivative into a TiO_2 Nanocrystalline Film Investigated by Visible-to-IR Ultrafast Spectroscopy. *J. Phys. Chem. B* **2005**, *109*, 16406–16414.
45. Haque, S. A.; Palomares, E.; Cho, B. M.; Green, A. N. M.; Hirata, N.; Klug, D. R.; Durrant, J. R. Charge Separation *versus* Recombination in Dye-Sensitized Nanocrystalline Solar Cells: The Minimization of Kinetic Redundancy. *J. Am. Chem. Soc.* **2005**, *127*, 3456–3462.
46. Nakade, S.; Kanzaki, T.; Kubo, W.; Kitamura, T.; Wada, Y.; Yanagida, S. Role of Electrolytes on Charge Recombination in Dye-Sensitized TiO_2 Solar Cell (1): The Case of Solar Cells Using the I^-/I_3^- Redox Couple. *J. Phys. Chem. B* **2005**, *109*, 3480–3487.
47. Fredin, K.; Nissfolk, J.; Boschloo, G.; Hagfeldt, A. The Influence of Cations on Charge Accumulation in Dye-Sensitized Solar Cells. *J. Electroanal. Chem.* **2007**, *609*, 55–60.
48. Piris, J.; Ferguson, A. J.; Blackburn, J. L.; Norman, A. G.; Rumbles, G.; Selmarten, D. C.; Kopidakis, N. Efficient Photoinduced Charge Injection from Chemical Bath Deposited CdS into Mesoporous TiO_2 Probed with Time-Resolved Microwave Conductivity. *J. Phys. Chem. C* **2008**, *112*, 7742–9.
49. Wang, P.; Zakeeruddin, S. M.; Comte, P.; Charvet, R.; Humphry-Baker, R.; Gratzel, M. Enhance the Performance of Dye-Sensitized Solar Cells by Co-Grafting Amphiphilic Sensitizer and Hexadecylmalonic Acid on TiO_2 Nanocrystals. *J. Phys. Chem. B* **2003**, *107*, 14336–14341.
50. Tachibana, Y.; Hara, K.; Sayama, K.; Arakawa, H. Quantitative Analysis of Light-Harvesting Efficiency and Electron-Transfer Yield in Ruthenium-Dye-Sensitized Nanocrystalline TiO_2 Solar Cells. *Chem. Mater.* **2002**, *14*, 2527–2535.